Experimental and Analytical Study of the Responses of Nanoscale Devices to Neutrons Impinging at Various Incident Angles

Golnaz Korkian, Juan Carlos Fabero, Guillaume Hubert, Mohammadreza Rezaei, Hortensia Mecha, Francisco J. Franco, Helmut Puchner and Juan A. Clemente

***Abstract*—In harsh radiation environments, it is well known that the angle of incidence of impinging particles against the surface of the operating devices has significant effects on their sensitivity. This paper discusses the sensitivity underestimations that are made if particle isotropy is not taken into account, by means of an analytical study made with a single event upset predictive platform. To achieve this goal, experimental results carried out with a COTS bulk 130-nm non-volatile SRAM for various incident angles on 14.2 MeV neutrons are firstly discussed. Then, a modeling tool called MUSCA-SEP3 is used to predict the sensitivity of this memory under the same environmental conditions. Predictions and experimental results will be cross-checked, therefore the feasibility of this tool will be demonstrated for testing any other incident angle. Finally, an isotropic environment and an XY SRAM array will be emulated with MUSCA in order to demonstrate that the asymmetrical cross-sections that were observed experimentally for various incidence angles are due to the underlying asymmetry of the metalization/passivation layers within the device with respect to its active silicon. Conclusions will finally be drawn as for the importance of taking into account particle isotropy in radiation-ground tests.**

***Index Terms*—COTS, SRAM, Neutron tests, Angle of incidence, SEU, MUSCA SEP3.**

I. Introduction and Related Work

RADIATION is a notable challenge for semiconductor technology. High-tech devices, from transistors to memories, deal with a plethora of so-called Single Event Upsets (SEUs), as well as other undesired phenomena [1]. Energetic particles such as neutrons and protons are the origin of said effects. These are typically classified as simple and multiple events. The former are usually known as Single Bit Upsets (SBUs), which occur when one particle flips only one cell. Otherwise, if the charge generated by impinging particles is shared by adjacent cells, this event is known as Multiple Cell Upset (MCU) and it is a significant issue resulting in corrupted data [1]–[3]. If the cells affected by a multiple event belong to the same word, the phenomenon becomes a Multiple Bit Upset (MBU) [2], [4].

One of the most important aspects that critically affects the signature and typology of the events observed under radiation is the incident angle of the particles against the surface of the device. Indeed, several studies in the literature have reported that impinging particles (coming from different sources of radiation) at large incident angles feature a higher probability of provoking MCUs and MBUs. Thus, it has been largely proven that heavy ions [5]–[7], low-energy protons [8]–[10] and neutrons [11]–[14] produce a strong angular dependence on SEU cross sections of modern microelectronic devices.

However, there are still limitations that researchers face when it comes to estimating and interpreting the SEU sensitivity of a device in a realistic environment when carrying out an accelerated test, some facilities like CERN emulate environments with isotropic particles, hence any angle of incidence is possible. However, in many others this is impossible, so researchers carry out tests by making particles hit the device at a single incidence angle, which is usually normal with respect to the device's surface [15]. This might lead to an underestimation of the actual sensitivity of the device in an actual environment. Thus, this paper proposes to explore angular effects and their contribution to the total SEU sensitivity through extensive analytical simulations.

For this purpose, a set of experiments on a Commercial-Off-The-Shelf (COTS) bulk non-volatile SRAM (nvSRAM), manufactured in 130-nm process, will be firstly presented as a case study. Two recent researches also focused on studying the radiation effects of heavy ions on this very same memory [16] and on a very similar one manufactured in 28-nm process [17]. However, this work focuses on understanding the above mentioned angular effects in an analytical way. These experiments involved 14.2 MeV neutrons at different angles of incidence: normal and grazing. Subsequently, the Multi-Scales Single Event Phenomena Predictive Platform (MUSCA-SEP3) [18] will be presented as a valid tool that is able to accurately predict the effects of various sources of radiation, including angular effects, on different semiconductor technologies. This tool can be used for predicting such effects on SRAMs, for any miniaturization level (not only 130-nm). This platform was developed by researchers of the Department of Physics (DPHY) at the ONERA research center, in Toulouse (France),

This work was supported in part by the Spanish MINECO project TIN2017-87237 and by the UCM mobility program for young professors.

G. Korkian, J. C. Fabero, M. Rezaei, H. Mecha, and J. A. Clemente are with the Computer Architecture Department, Facultad de Informática, Universidad Complutense de Madrid (UCM), Spain, e-mail: {gkorkian, jcfabero, horten, mrezaei, juanancl}@ucm.es.

G. Hubert is with the ONERA French Aerospace Laboratory, Toulouse, France, email: guillaume.hubert@onera.fr.

F. J. Franco is with the Department of Structure of Matter, Thermal Physics, and Electronics, and also with Institue of Particle and Cosmos Physics (IPARCOS), Facultad de Ciencias Físicas, Universidad Complutense de Madrid (UCM), Spain, e-mail: fjfranco@fis.ucm.es.

H. Puchner is with Cypress Semiconductor, Technology R&D, 3901 San Jose, CA, USA. e-mail: hrp@cypress.com.

and it performs Monte Carlo simulations that emulate the transport of radiation through matter [19].

The main goal of this research is to give more insight about the nuclear mechanisms behind this phenomenon, and to demonstrate that such angular effects can be accurately predicted with the above mentioned predictive tool. In particular, the following points will be discussed:

1) An isotropic environment and an XY SRAM array will be emulated with MUSCA-SEP3. Experiments taken as a case study will be cross-checked with first-order SEU sensitivity predictions.
2) The nuclear mechanisms (neutron-nucleus reactions) leading to the difference between SEU cross-sections at different angles will be discussed. Directions and penetration range of secondary ions will be provided.
3) A thorough SEU sensitivity assessment in environments with isotropic particles will be finally made with MUSCA-SEP3.

The remainder of the paper is organized as follows: Section II describes the experimental setup and the target device that was used as a case study. Next, Section III discusses the experimental results. Section IV uses the MUSCA-SEP3 tool in order to provide justifications of the angular effects observed experimentally. An analytical study of the SEU sensitivity of the device at a plethora of angles of incidence is also presented in that section. Finally, conclusions are drawn in Section V.

II. Experimental Setup

Experimental tests were carried out in May 2018 on the CY14V101QS COTS nvSRAM, which has a capacity of 1 Mbit. This part is manufactured by Cypress semiconductor. The memory is organized as two layers of 1 Mb, one consisting of 130-nm CMOS SRAM and the other one, nonvolatile SONOS[1] Quantum Trap cells[2]. At power down, the data on the SRAM layer automatically is transferred to the nonvolatile one. At power up, data are restored to the SRAM from the nonvolatile layer [20]. During the tests, the device always operated at nominal voltage. The memory is accessed through a Serial Peripheral Interface (SPI) and read/write operations are carried out at a clock frequency that can reach up to 108 MHz. The SRAM layer is manufactured in 130-nm bulk CMOS technology [20]. This memory features bit interleaving, which has been unscrambled by using proprietary information provided by the manufacturer.

The test system (Fig. 1) comprised an Arduino DUE, which runs the test software, and an extension board with the memory under test. An additional control computer was responsible for the data retrieval. The Arduino communicates with the control computer through a UART, whereas the ARM Cortex-M3 microcontroller of the Arduino communicates with the SRAM through the SPI. In order to obtain reliable results, all the elements of the setup existing in the irradiation chamber were shielded with thick polyethylene plates except the DUT.

[1]Short for Silicon - Oxide - Nitride - Oxide - Silicon

[2]The embedded nonvolatile elements integrate the so-called "Quantum Trap" cells, generating reliable storage of data

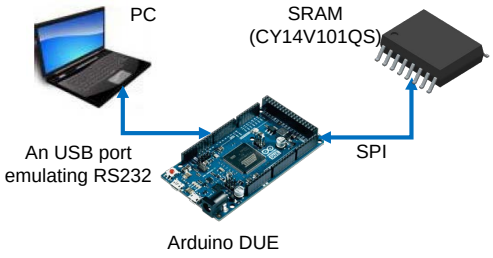

Fig. 1. Experimental setup for the tests

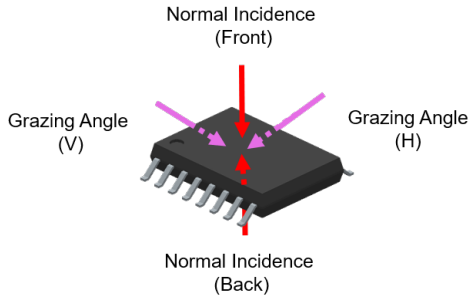

Fig. 2. Beam incident angles that were tested

The tests were run at the GENEPI2 neutron source, which is operated at the LPSC (Laboratoire de Physique Subatomique et de Cosmologie) in Grenoble (France) [21], [22]. This accelerator is under operation on the GENESIS platform (GEnerator of NEutrons for Science and IrradiationS). GENEPI2 is an electrostatic accelerator producing neutrons by impinging a deuteron beam onto a fixed target. With a Tritium (T) target, neutrons are produced via the nuclear fusion reaction ${}^{2}_{1}d+{}^{3}_{1}T \rightarrow {}^{1}_{0}\,n+{}^{4}_{2}He$ with an average energy of 14.2 MeV. An ion source, operating at the electronic cyclotronic resonance, produces an intense and continuous deuterium (d) ion beam. A series of electrodes shape the beam, which is accelerated to 220 keV through an electrostatic column. After magnetic selection by a dipolar electromagnet, deuterons are guided through a 5 meter long transport line, including focusing and steering elements. The beam line terminates with the target made of a tritium compound. From the production target, neutrons are emitted in all directions. For the radiation tests, the devices under test are set facing directly the tritium target, at a small distance determined according to the required neutron flux. The neutron production is monitored continuously throughout experiments to determine the dose for each irradiation (accuracy better than $\pm 15\%$).

Static tests were carried out: the memory was initialized to a pattern, then it was irradiated while keeping it idle and finally errors were checked after having stopped the radiation beam. Rounds from 1 to 10 minutes were carried out, at fluxes that ranged from 1.04×10^7 to $9.70 \times 10^7 \mathrm{n} \cdot \mathrm{cm}^{-2} \cdot \mathrm{s}^{-1}$. The memory was irradiated with 2 different incident angles (normal and grazing) and for each one of them, two directions were tested. These are depicted in Fig. 2: horizontal (H) and vertical (V) for grazing angles; and the front and back of the memory for normal incidence.

TABLE I
ROUNDS OF IRRADIATION PERFORMED ON STATIC EXPERIMENTS

N^o	Angle	Distance test (cm)	Pattern	Fluence ($\times 10^{10}$) (n/cm^2)	Number of affected addresses
1	Normal incidence (Front)	1.9	0x55	2.34	902
2		1.9	0x55	2.34	914
3		1.9	0x55	4.65	1810
4		1.9	0xFF	2.33	938
5		1.9	0xFF	2.34	899
6		1.9	0x00	2.32	904
7		1.9	0x00	2.32	860
8		1.9	0xAA	2.33	949
9		1.9	0xAA	2.32	955
10	Grazing angle (H)	2.6	0x55	1.24	588
11		2.6	0xFF	1.24	649
12		2.6	0xAA	1.23	574
13		2.6	0x00	1.25	626
14	Grazing angle (V)	3.2	0x55	0.818	338
15		3.2	0xFF	0.818	378
16		3.2	0xAA	0.818	335
17		3.2	0x00	0.826	339
18	Normal incidence (Back)	5.2	0x55	0.62	177
19		5.2	0x55	0.78	221
20		5.2	0xAA	0.776	226
21		5.2	0xFF	0.777	239
22		5.2	0x00	0.778	241

In Section IV, MUSCA-SEP3 [18] will be used to validate and to give a further interpretation of these results. This tool has as input a XY floorplan of memory cells, without taking into account any other on-chip architectural module, such as I/O buffers, row/column decoders, sense amplifiers, etc. Static tests will only be considered for this reason. Besides, the study of the sensitivity during dynamic tests due to angular effects would require profound modifications in MUSCA, which unfortunately is not possible now, so it will not studied in this paper.

III. EXPERIMENTAL RESULTS

A. Discussion of SBUs and MCUs

Tests with different patterns written in the memory were made (0x00, 0xFF, 0x55 and 0xAA). Such different patterns were used in order to check whether or not there is any correlation between the MCU abundance and said pattern, for any of the tested angles.

Table I shows the rounds of irradiation that were carried out, grouped into 16 different types of experiments (4 patterns x 2 incident angles x 2 directions). Each round of reading had its particular flux, distance and exposure time. For the grazing angles, the distance was calculated to the center of the chip. These are different because the extension board was not symmetric, hence these numbers are actually forced and not chosen. Roughly, it can be observed that the number of affected addresses is similar in all the rounds of irradiation that had similar fluence. They also seem to scale accordingly with said fluence. The errors discussed in this section will correspond to the bulk CMOS layer of the nvSRAM.

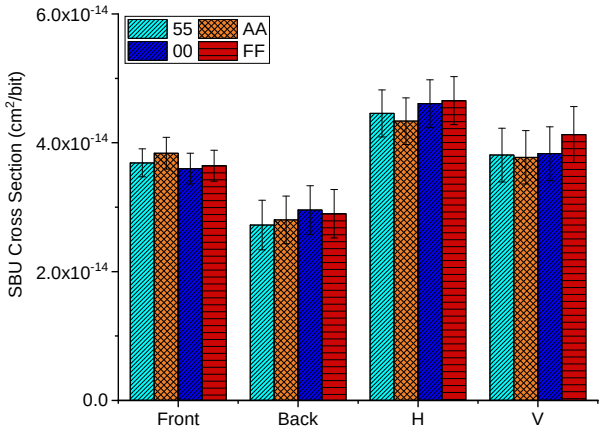

Fig. 3. Experimental SBU cross sections obtained at different incident angles and patterns

Subsequently, SBUs and MCUs must be extracted from the set of detected SEUs in order to carry out a correct analysis of the SEU sensitivities depending on the multiplicity of the events. This was done by using unscrambling proprietary information provided by Cypress Semiconductor, which allowed translating the logical addresses into physical ones. This made possible to find the physical XY cell placement of the errors in the SRAM. Once the placement was found, it was postulated that bitflips in two different cells were provoked by the impact of the same particle (and thus, they were part of the same multiple event) if the Manhattan distance [23] between both of them is less than or equal to D_{MAX}. This parameter must be selected by the researchers (in this case, this value was 2). In addition, according to Table I, in some rounds of reading the number of recorded bitflips was high, hence the probability of a multiple event being the result of 2 simple ones is not negligible. For this reason, the equations presented by the authors in [24] were used to correct the numbers of MCUs that were primarily found. These equations were also used to discuss the so-called false MBUs, which will be discussed in the next subsection.

Fig. 3 shows the SBU cross sections for different patterns and angles, the error margins of which have been calculated with 95% confidence, as explained in [25], [26]. It is observed that the SBU sensitivity increases at grazing angles, and that the H direction showed to be more prone against SBUs for all the patterns. It can be observed that, for a normal incidence, the irradiation from the back yielded fewer errors (therefore, a lower sensitivity) than from the front. The physical mechanisms leading to this phenomenon will be deeply discussed in Section IV.

Next, Fig. 4 shows the experimental 2-bit MCU cross sections. In this case, fewer events were observed. This figure shows a similar trend to Fig. 3. On the one hand, the higher error rates observed at grazing angles (H and V) are consistent with the experimental results presented by Harada *et al.* [27], Hirokawa *et al.* [13] and Kato *et al.* [12], where it is also pointed out that the sensitivity for 2-bit MCUs increases at grazing angles. On the other hand, again in this figure it is

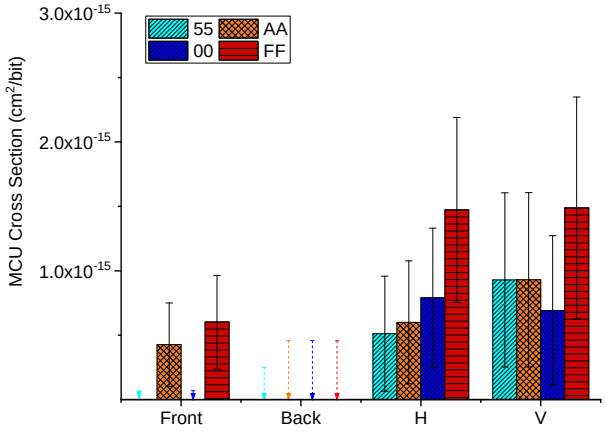

Fig. 4. Experimental 2-bit MCU cross sections obtained at different incident angles and patterns. Arrows indicate the uppermost possible values for cross section in this memory if no events were observed. These were calculated assuming that 3.69 is the uppermost possible number of events with 95% confidence if no event was observed [25]

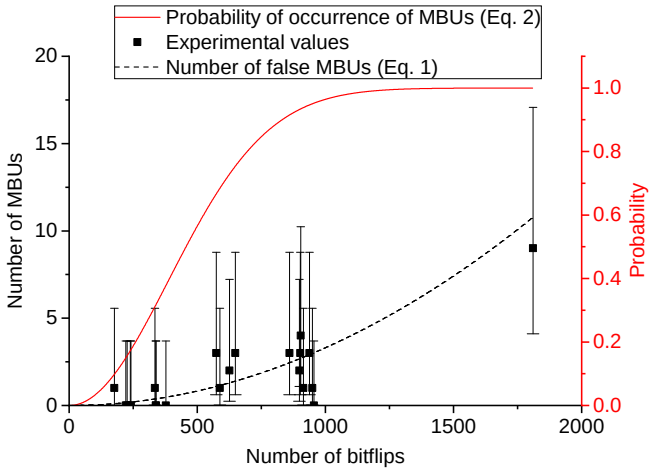

Fig. 5. Experimental and estimated number of 2-bit MBUs (dots and (1) - dashed line). The continuous line indicates the probability of occurrence of 2-bit MBUs according to (2)

observed that the number of events increases when irradiating from the front of the SRAM, in comparison with receiving the radiation from the back. It should be mentioned that very few MCUs were observed at normal incidence (Front & Back). However, the abundance of these was considerably higher for grazing ones (H & V).

Section IV will provide a detailed justification of why this happens, by using the MUSCA-SEP3 prediction tool. Finally, the large confidence margins make it difficult to reach further conclusions, particularly regarding the dependence on the pattern (constant or *checkerboard*).

B. Discussion of MBUs

Due to the large number of observed bitflips, as well as the relatively small size of the memory (only 1 Mb), the chance of observing pairs of nearby but independent SBUs and of confusing them with multiple events is not negligible. Since the DUT implemented bit interleaving, it is not possible that a single particle provokes an MBU. However, during the experiments, several 2-bit MBUs were observed, presumably due to the accumulation of 2 SBUs in the same word.

Let us apply techniques to predict the number of false MBUs. For that purpose, we will use a model developed by the authors in a previous work [28], to estimate the expected number of so-called *"false"* 2-bit MBUs by accumulation. It is compatible with the well-known birthday statistics model [29] and this is a good opportunity to back it up with more experimental data. Thus, the expected number of false 2-bit MBUs would be ((9) in [28]):

$$N_{\mathrm{F\_2bit\_MBU}} = \frac{1}{2} \cdot \frac{W-1}{W} \cdot \frac{m \cdot (m-1)}{L_{\mathrm{A}}} \cdot \left(1 - \frac{m-2}{L_{\mathrm{A}}}\right) \quad (1)$$

W being the wordwidth (8 bits), m the number of bitflips and L_{A} the memory size in words. The second study was done by Tausch's prediction [30] on Error Detection And Correction (EDAC) techniques.

Fig. 5 shows the number of experimental 2-bit MBUs (dots and confidence margins) in comparison with the predictions issued by (1) (dashed line). Dots refer to the different rounds that were made (Table I). The prediction reasonably matches all the experimental occurrences that were noticed, which allows reaching the conclusion that the experimental MBUs were actually false ones. The figure also includes the probability of occurrence of such multiple events continuous line, which obviously tends to 1 as the number of affected addresses increases. This probability was taken from (17) in [30] and it can be modeled as follows:

$$\mathrm{PROB}_k(n,m)_{\mathrm{2bit\_MBU}} \approx 1 - exp(-\frac{m \cdot (m-1) \cdot (2k-1)}{2n}) \quad (2)$$

where n is the memory size in bits (in this case, 2^{20}), m is the number of bitflips and k is a value postulated by the authors to be set to $\frac{W}{2}$. Note that both lines (continuous and dashed) refer to different vertical scales (right and left, respectively).

IV. SEU Sensitivity Assessment with MUSCA SEP3

In this section, the SEU predictive platform MUSCA-SEP3 [18], [31], [32] will be used for understanding the nuclear mechanisms that explain the angular effects in the experimental cross-sections presented in Section III. More specifically, energies and directions of secondary ions produced by the neutron-nucleus reactions will be discussed. Finally, this tool will be used to extrapolate to a realistic environment, where a plethora of angles of incidence is possible.

MUSCA-SEP3 is a Monte Carlo prediction tool that, working with databases, is able to simulate the radiation effects of different kinds of particles (protons, neutrons, heavy ions...) on memories implemented with diverse semiconductor manufacturing technologies (bulk CMOS, SOI, Fin-FET, etc), taking into account the miniaturization of the technological node. It provides a complete simulation environment that models the interaction of the radioactive particles with the matter,

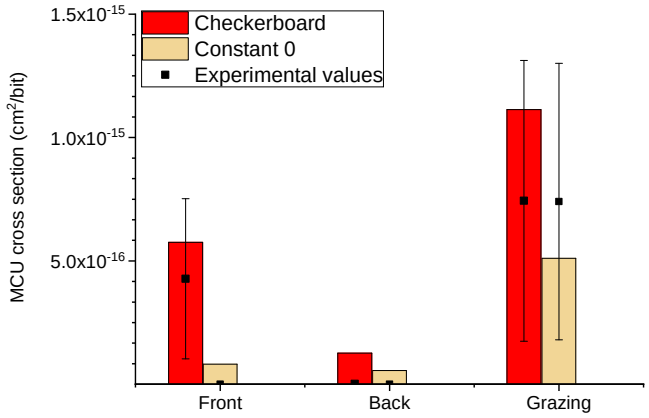

Fig. 6. Comparison of 2-bit MCU cross sections issued from MUSCA SEP3 vs. experimental results for different incidence angles and patterns.

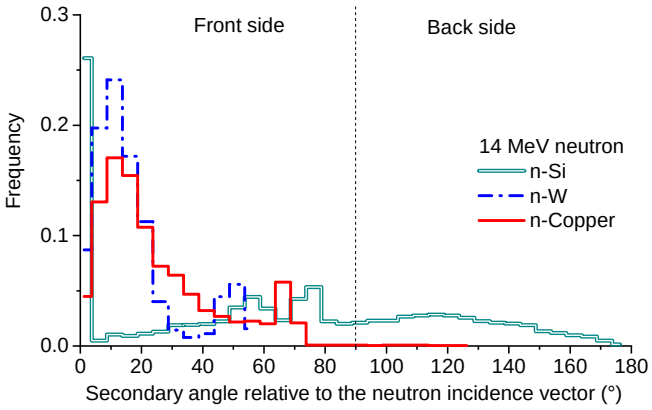

Fig. 7. Emission angle frequency of secondary ions induced by a 14.2 MeV neutron interaction with Silicon, Tungsten and Copper ion nuclei. The incidence (or direction) vector of neutrons in this simulation is normal with respect to the device's surface

which allows performing estimations of the SEU sensitivity, from the overall system down to the semiconductor level. MUSCA SEP3 receives as inputs a device description, the semiconductor active zones, and critical charge of the bit cells without the need for any particular experimental data [18].

For the case of modeling a SRAM with MUSCA-SEP3, the elementary cell is firstly described, so the rules of translation are applied to all the memory. For modeling the elementary cell, several volumes are used to represent physical sensitive drains; i.e., their sizes, and positions. To illustrate the methodology of modeling of the studied SRAM (planar bulk technology), the active zones (drains and sources) and the Shallow-Trench Isolation (STI) topology are designated. In this technique, a General Design Specification (GDS) extractor is used to get these details from GDSII files. Reverse engineering leads to the detailed knowledge of the elementary cell topology. Furthermore, this reverse analysis obtains the crucial physical parameters of the device such as NMOS and PMOS drains implantation and the metallization and the passivation layers [33].

A. SEU Sensitivity Trends vs. Pattern and Angle

In order to validate the pertinence of MUSCA-SEP3, simulations issued from this tool are compared with the experimental ones. Fig. 6 shows such comparison, for 2-bit MCUs. Since the experimental results were not conclusive about the correlation between the pattern and the device SEU sensitivity, the figure only displays averaged results regarding both *checkerboard* and the "Constant 0" patterns ("Constant 1" is not shown for simplicity). Columns display predictions, whereas dots do likewise with experimental results (again, with 95% confidence margins). Two conclusions can be drawn:

- Predictions show a good concordance with the experimental results, including a lower sensitivity in neutron tests made from the back of the device.
- Predictions do depict a slight dependence on the pattern (the sensitivity seems to be lower for the "Constant 0" pattern). As discussed above, this point could not be confirmed by just looking at the experimental results.

B. MUSCA-SEP3 Analytical Study of Angular Effects

The objective of this subsection is to further understand the nuclear mechanisms leading to the difference between SBU and MCU cross sections observed both experimentally and in MUSCA-SEP3 simulations, regarding the different angles of incidence that were tested in the experiments.

For 14.2 MeV neutrons, the impact in semiconductor devices is predominantly caused by nuclear neutron scattering processes. Recoil atoms, commonly referred to as "primary knock-on atoms" (PKAs) are produced through neutron-nucleus interactions and they traverse the device materials, including passivation, metallization and the active semiconductor. Secondary ions are characterized by their atomic numbers, mass numbers, energies and directions.

From the strict point of view of nuclear interaction, back-side or front-side irradiations imply the same secondary ion productions, with very similar characteristics. These, in turn, create electron-hole pairs in the active silicon that participate in the transport and charge collection mechanisms. However, the metallization and the passivation layers of the device are asymmetrically distributed with respect to the active silicon substrate (i.e., they exist in the front side, but not in the back side), whereas the active silicon is symmetrically distributed with respect to itself. Thus, angular properties may be suspected of having a significant impact on the SEU occurrence, and in particular, for 14.2 MeV neutrons.

In order to get a deeper insight about this, the characteristics of secondary particles including elastic and non-elastic reactions in Silicon (Si), Tungsten (W) and Copper (Cu) have been investigated using Geant4 simulations [34]. In silicon, secondary ions can range from H to P with several isotopes. In this work, on the order of 10^4 interactions were considered for these three species. Simulations provide the secondary ions count, atomic and mass numbers, their energies and directions. Fig. 7 presents the emission angle frequency for the three species, which is measured with respect to the neutron direction vector (featuring normal incidence with respect to the device's surface). The figure only shows the abundance of secondary ions whose energy is high enough to participate

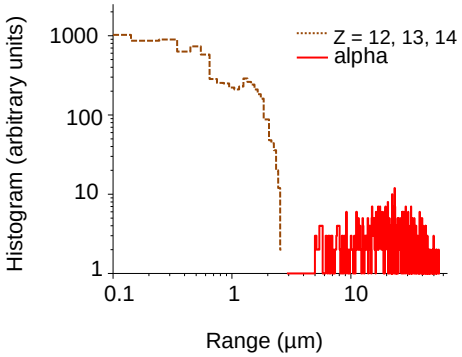

Fig. 8. Distribution of secondary ion range (Z > 11) and alpha particles, for which the LET value is greater than $0.1\mathrm{MeV}\cdot\mathrm{cm}^2/\mathrm{mg}$

in the SEE generation process (a minimum threshold value of 0.1MeV was considered for this purpose). Angle values ranging 0° to 90° correspond to secondary ions emitted in the direction of the incident vector, whereas angles greater than 90° imply secondary ions emitted in the opposite direction. Results presented in the figure show that, for 14.2 MeV neutron interactions, secondary ions are mainly emitted in the direction of the neutron incident vector. This is especially true for n-W and n-Cu interactions, which reinforces the idea that the secondary ions emitted by these reactions explain the differences between SEE sensitivities in front neutron incidence vs. back. Complementary analyses show that secondary alpha and proton angular emission is close to an isotropic one.

Therefore, the front-side irradiation is characterized by the contribution to the SEU cross sections of secondary ions produced in the active silicon and the passivation/metallization layers. However, in the case of the back-side irradiation, secondary ions produced in the passivation/metallization layers participate sparsely to the generation of electron-hole pairs in the active silicon. In fact, only 0.48% and 33.5% of secondaries are emitted backwards from n-Cu and n-Si reactions, respectively. This explains the significant difference that was observed (both experimentally and through simulations) between the SEU sensitivities of both kinds of tests.

In the case of lateral irradiation, the interpretation is more complex. When a neutron traverses the active zones of the device from the front or the back, the effective thickness that participates to the SEU occurrence via the nuclear processes is in the order of 10 to 20 μm. However, in the case of lateral incidence, the sensitive areas correspond to the whole SRAM array.

In Fig. 7, an analysis of secondary ions induced by 14.2 MeV neutron interactions showed that they are mainly emitted in the direction of the neutron incidence angle. In the case of front/back incidence, the occurrence of MCUs is due to the proximity of the carrier deposition on adjacent cells and/or the carrier diffusion mechanism. However, in the case of lateral incidence, the path of the particle may impact a larger number of cells, which strongly depends on the coupled secondary ion range and carrier density. Thus, Fig. 8 presents the distribution of secondary ion range for which the LET value is greater than

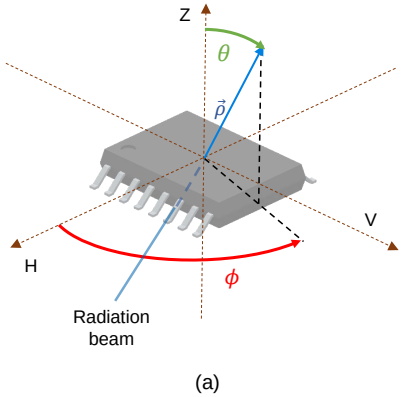

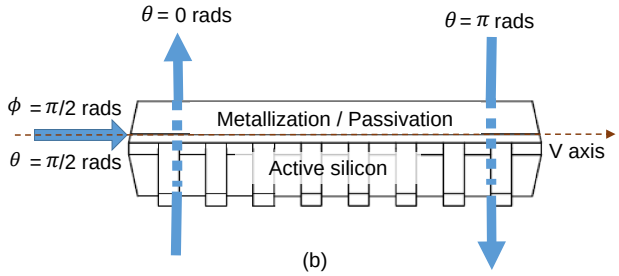

Fig. 9. a) Spherical coordinate system and b) passivation / metallization layers. θ and ϕ are the tilt angles of the incident particles with respect to the Z and H axis, respectively

$0.1\mathrm{MeV}\cdot\mathrm{cm}^2/\mathrm{mg}$ (i.e. $\sim 1\mathrm{fC}/\mu\mathrm{m}$ corresponding to the order of magnitude of the upset threshold). Results are presented for heavy ions (Z > 11) and alpha particles. Concerning the latter, range values are on the order of few tens of micrometers (note the logarithmic scale), which confirm that the track of the particle can match, or be very similar to, the thickness of the plane of the SRAM array. Obviously, this is only possible in the case of a lateral incidence. For heavy secondary ions, the range value can be greater than 1 μm, with a significant carrier generation in several adjacent cells. In any case, this figure shows that the lateral incidence is more favorable to the occurrence of multiple events.

C. Assessment of SEU Sensitivity in Environments with Isotropic Particles

This subsection investigates the influence of the angular properties on the SEU sensitivity. The previous subsection has shown that the SBU and MCU cross sections issued by MUSCA-SEP3 are accurate in comparison to the the experimental ones, considering the front, back, and lateral incidence. Thus, simulations can be applied for other incidences, using a spherical description based on the θ and ϕ angles, as depicted in the spherical coordinate system of Fig. 9(a). Vector $\overrightarrow{\rho}$ defines the direction and sense of incidence of the radiation beam, whereas θ is the angle with respect to the Z axis, and ϕ is the angle of the projection of $\overrightarrow{\rho}$ on the HV plane concerning the H axis. Note that the H and V axes are consistent with the simplified description of the directions given in Fig. 2. Fig. 9(b) depicts the position of the passivation / metallization

TABLE II
2-BIT MCU CROSS SECTIONS (cm^2/bit), OBTAINED WITH MUSCA-SEP3, AS A FUNCTION OF θ AND ϕ (SEE FIG. 9), WITH AN ANGULAR RESOLUTION OF $\frac{\pi}{4}$ AND $\frac{\pi}{8}$, RESPECTIVELY. IN LIGHT-GRAY CELLS, THE FRONT, BACK AND GRAZING INCIDENCES DISCUSSED IN SECTION III. THE DARK-GRAY CELL IS THE HIGHEST VALUE

		ϕ (rads)				
		0	$\frac{\pi}{8}$	$\frac{\pi}{4}$	$\frac{3\cdot\pi}{8}$	$\frac{\pi}{2}$
θ (rads)	0	5.61	5.61	5.61	5.61	5.61
	$\frac{\pi}{4}$	7.2	7.93	9.83	8.36	7.9
	$\frac{\pi}{2}$	38.3	45.7	62.3	56.8	51.1
	$\frac{3\cdot\pi}{4}$	10.5	11.5	14.3	12.2	11.5
	π	8.16	8.16	8.16	8.16	8.16
		$\times 10^{-17} cm^2/bit$				

layers over the sensitive volume of silicon. It should be said that $\theta = 0$ makes $\overrightarrow{\rho}$ point to the back of the board and $\theta = \pi$ corresponds to the front of the board.

Table II and Fig. 10 present the MCU cross sections for 14.2 MeV neutrons as a function of θ and ϕ, with an angular resolution of $\pi/4$ and $\pi/8$, respectively by means of MUSCA SEP3. For simplicity, θ ranges from 0 to π and ϕ ranges from 0 to $\pi/2$. Therefore, only a quarter of the possible angles of θ and ϕ has been simulated, which corresponds to the sector that is facing the reader in Fig. 9(a).

In this case, it is interesting to note that the worst configuration was obtained for $\theta = \pi/2$ and $\phi = \pi/4$, i.e. an oblique grazing direction (see Fig. 10 in between H and V) that maximizes the SEE sensitivity (both off-state transistors simultaneously impacted by the charge deposition). In fact, this maximum value ($6.23 \times 10^{-16} cm^2/bit$) and the minimum one ($5.61 \times 10^{-17} cm^2/bit$) differ by one order of magnitude.

It also has to be noted that the grazing incidences discussed in the previous section are amongst the highest sensitivities simulated in this study, albeit none of them is the absolute highest one. They correspond to the cells ($\theta = \pi/2$, $\phi = 0$) and ($\theta = \pi/2$, $\phi = \pi/2$). These ones, as well as the front and back incidences, have been highlighted in light-gray color in the table for the sake of clarity. Also, note that, when keeping θ constant to $\pi/2$ (grazing direction always parallel to the HV plane), changing ϕ leads to an asymmetrical variation of the MCU sensitivity, which is higher towards the V direction ($\theta = \phi = \pi/2$).

Thus, for instance, for 2-bit MCUs, the device sensitivity can be calculated considering two hypotheses:

- Front normal incidence of the neutrons with an MCU cross-section of $5.61 \times 10^{-17} cm^2/bit$. This is a clear underestimation when considering the results of Table II and Fig. 10.
- Isotropic incidence of the neutrons. This case implies integrating the product of neutron fluence and 2-bit MCU cross section over the solid angle. In this case, considering that 1) these results can be extrapolated to the rest of possible incident angles ($\theta = \{\pi \cdots 2\pi\}$ and $\phi = \{\pi/2 \cdots 2\pi\}$), 2) all the possible incident angles have the same probability, and 3) keeping the angular resolution of Table II, the estimated sensitivity would be around $1.70 \times 10^{-16} cm^2/bit$, which more than doubles the one that would be considered in an anisotropic environment where only normal incidence is taken into account.

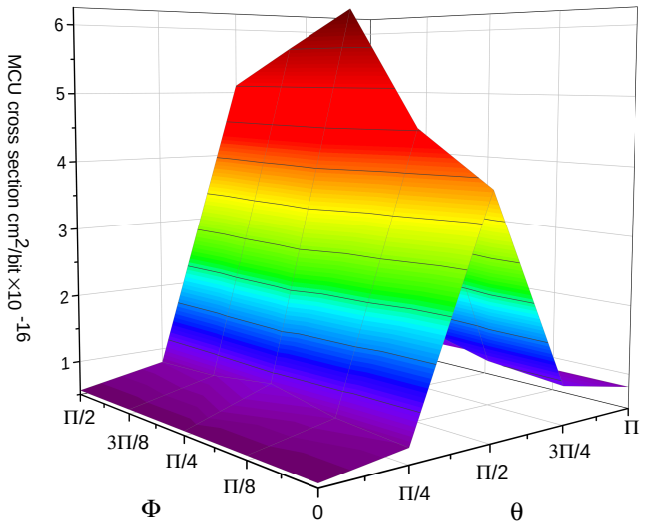

Fig. 10. 2-bit MCU cross sections (cm^2/bit), obtained with MUSCA-SEP3, of the tested technology (130-nm bulk CMOS), as a function of θ and ϕ angles of incidence. Graphical representation of the data of Table II

Of course, this approach is valid for any other technologies (Fin-FET, SoI, etc...) and miniaturization nodes. Additionally, this study remains valid for non-interleaved architectures (such as old FPGAs), where part of the MCUs will actually be MBUs provoked by a single particle. These conclusions can be considered as a first step towards the analysis of other memories operating in harsh environments.

V. CONCLUSIONS

This paper has provided an interpretation of the nuclear mechanisms (neutron-nucleus) that explain the SEU sensitivity differences in nanoscale devices when they are hit by particles impinging at different angles of incidence. For this purpose, the predictive platform MUSCA-SEP3 has been used. Firstly, the accuracy of this tool to predict cross-sections taking angular effects into account has been discussed. To attain this objective, first-order simulations were cross-checked with experimental results obtained with 14.2 MeV neutrons on a bulk 130-nm SRAM. Both simulations and predictions showed good concordance. Then, this tool was used to provide more insight about the physical reasons that explain this phenomenon, namely the directions and penetration range of secondary ions produced in the nuclear reactions, and the asymmetry of the metalization/passivation layers of the device with respect to its active silicon. Finally, an isotropic environment on an XY SRAM array was thoroughly emulated, thereby quantifying the SEU sensitivity divergence among different neutron incident angles.

ACKNOWLEDGEMENT

The authors are very grateful to our colleagues S. Rey, T. Gemond and M. Baylac, from the Laboratoire de Physique

Subatomique et Cosmologie LPSC, Université Grenoble-Alpes & CNRS/IN2P3. The work on GENEPI2 at LPSC (CNRS/UGA) has been performed within the "Characterisation Program" of the IRT nanoelec, co-funded by the french governement in the frame of the so called "Programme d'Investissements d'Avenir" under the reference ANR-10-AIRT-05.

REFERENCES

[1] J. A. Clemente *et al.*, "Statistical Anomalies of Bitflips in SRAMs to Discriminate SBUs From MCUs," *IEEE Transactions on Nuclear Science*, vol. 63, no. 4, pp. 2152–2160, 2016.

[2] A. Bosser *et al.*, "Investigation on MCU Clustering Methodologies for Cross-Section Estimation of RAMs," *IEEE Transactions on Nuclear Science*, vol. 62, no. 6, pp. 2620–2626, 2015.

[3] G. Tsiligiannis *et al.*, "Multiple Cell Upset Classification in Commercial SRAMs," *IEEE Transactions on Nuclear Science*, vol. 61, no. 4, pp. 1747–1754, 2014.

[4] M. Wirthlin, D. Lee, G. Swift, and H. Quinn, "A Method and Case Study on Identifying Physically Adjacent Multiple-Cell Upsets Using 28-nm, Interleaved and SECDED-Protected Arrays," *IEEE Transactions on Nuclear Science*, vol. 61, no. 6, pp. 3080–3087, 2014.

[5] J. M. Hutson *et al.*, "Evidence for Lateral Angle Effect on Single-Event Latchup in 65 nm SRAMs," *IEEE Transactions on Nuclear Science*, vol. 56, no. 1, pp. 208–213, 2009.

[6] A. D. Tipton *et al.*, "Device-Orientation Effects on Multiple-Bit Upset in 65 nm SRAMs," *IEEE Transactions on Nuclear Science*, vol. 55, no. 6, pp. 2880–2885, 2008.

[7] D. S. Lee, G. M. Swift, M. J. Wirthlin, and J. Draper, "Addressing Angular Single-Event Effects in the Estimation of On-Orbit Error Rates," *IEEE Transactions on Nuclear Science*, vol. 62, no. 6, pp. 2563–2569, 2015.

[8] N. A. Dodds *et al.*, "The Contribution of Low-Energy Protons to the Total On-Orbit SEU Rate," *IEEE Transactions on Nuclear Science*, vol. 62, no. 6, pp. 2440–2451, 2015.

[9] D. F. Heidel *et al.*, "Low Energy Proton Single-Event-Upset Test Results on 65 nm SOI SRAM," *IEEE Transactions on Nuclear Science*, vol. 55, no. 6, pp. 3394–3400, 2008.

[10] N. Ikeda, S. Kuboyama, S. Matsuda, and T. Handa, "Analysis of angular dependence of proton-induced multiple-bit upsets in a synchronous SRAM," *IEEE Transactions on Nuclear Science*, vol. 52, no. 6, pp. 2200–2204, 2005.

[11] A. D. Tipton *et al.*, "Increased Rate of Multiple-Bit Upset From Neutrons at Large Angles of Incidence," *IEEE Transactions on Device and Materials Reliability*, vol. 8, no. 3, pp. 565–570, 2008.

[12] T. Kato, T. Yamazaki, N. Saito, and H. Matsuyama, "Neutron-Induced Multiple-Cell Upsets in 20-nm Bulk SRAM: Angular Sensitivity and Impact of Multiwell Potential Perturbation," *IEEE Transactions on Nuclear Science*, vol. 66, no. 7, pp. 1381–1389, 2019.

[13] S. Hirokawa, R. Harada, M. Hashimoto, and T. Onoye, "Characterizing Alpha- and Neutron-Induced SEU and MCU on SOTB and Bulk 0.4-V SRAMs," *IEEE Transactions on Nuclear Science*, vol. 62, no. 2, pp. 420–427, 2015.

[14] S. Abe, W. Liao, S. Manabe, T. Sato, M. Hashimoto, and Y. Watanabe, "Impact of Irradiation Side on Neutron-Induced Single-Event Upsets in 65-nm Bulk SRAMs," *IEEE Transactions on Nuclear Science*, vol. 66, no. 7, pp. 1374–1380, 2019.

[15] S. Duzellier *et al.*, "Radiation Testing of Electronics Systems: How Can Simulation Tools Help in the Definition and Optimization of Test Plans in Labs?," *Aerospace Lab*, no. 12, pp. 1–9, 2016.

[16] T. Liu *et al.*, "Heavy Ion Radiation Effects on a 130-nm COTS NVSRAM Under Different Measurement Conditions," *IEEE Transactions on Nuclear Science*, vol. 65, no. 5, pp. 1119–1126, 2018.

[17] N. Rezzak, J. Wang, S. Varela, G. Bakker, and A. N. Gu, "Neutron and Proton Characterization of Microsemi 28 nm PolarFire SONOS-Based FPGA," in *2018 IEEE Radiation Effects Data Workshop (REDW)*, 2018.

[18] G. Hubert, S. Duzellier, C. Inguimbert, C. Boatella-Polo, F. Bezerra, and R. Ecoffet, "Operational SER Calculations on the SAC-C Orbit Using the Multi-Scales Single Event Phenomena Predictive Platform (MUSCA SEP^3)," *IEEE Transactions on Nuclear Science*, vol. 56, no. 6, pp. 3032–3042, 2009.

[19] R. A. Reed *et al.*, "Anthology of the Development of Radiation Transport Tools as Applied to Single Event Effects," *IEEE Transactions on Nuclear Science*, vol. 60, no. 3, pp. 1876–1911, 2013.

[20] Cypress Semiconductor, "CY14V101QS, 1-Mbit (128K×8) Quad SPI nvSRAM." Online. Available at http://www.cypress.com/file/178606/download, 2017.

[21] F. Villa *et al.*, "Accelerator-Based Neutron Irradiation of Integrated Circuits at GENEPI2 (France)," in *2014 IEEE Radiation Effects Data Workshop (REDW)*, pp. 1–5, 2014.

[22] F. Villa *et al.*, "Multipurpose applications of the accelerator based neutron source GENEPI2," *Nuovo Cimento C Geophysics Space Physics C*, vol. 38, article no. 182, 2016.

[23] S. Craw, *Manhattan Distance*, pp. 639–639. Boston, MA: Springer US, 2010.

[24] F. J. Franco, J. A. Clemente, G. Korkian, J. C. Fabero, H. Mecha, and R. Velazco, "Inherent Uncertainty in the Determination of Multiple Event Cross Sections in Radiation Tests," *IEEE Transactions on Nuclear Science*, vol. (in press), 2020.

[25] J. L. Autran, D. Munteanu, P. Roche, and G. Gasiot, "Real-time soft-error rate measurements: A review," *Microelectronics Reliability*, vol. 54, no. 8, pp. 1455 – 1476, 2014.

[26] R. Velazco *et al.*, "Evidence of the Robustness of a COTS Soft-Error Free SRAM to Neutron Radiation," *IEEE Transactions on Nuclear Science*, vol. 61, no. 6, pp. 3103–3108, 2014.

[27] R. Harada, S. Abe, H. Fuketa, T. Uemura, M. Hashimoto, and Y. Watanabe, "Angular Dependency of Neutron-Induced Multiple Cell Upsets in 65-nm 10T Subthreshold SRAM," *IEEE Transactions on Nuclear Science*, vol. 59, no. 6, pp. 2791–2795, 2012.

[28] F. J. Franco, J. A. Clemente, H. Mecha, and R. Velazco, "Influence of Randomness During the Interpretation of Results From Single-Event Experiments on SRAMs," *IEEE Transactions on Device and Materials Reliability*, vol. 19, no. 1, pp. 104–111, 2019.

[29] M. Abramson and W. O. J. Moser, "More Birthday Surprises," *The American Mathematical Monthly*, vol. 77, no. 8, pp. 856–858, 1970.

[30] H. J. Tausch, "Simplified Birthday Statistics and Hamming EDAC," *IEEE Transactions on Nuclear Science*, vol. 56, no. 2, pp. 474–478, 2009.

[31] G. Hubert *et al.*, "Continuous High-Altitude Measurements of Cosmic Ray Neutrons and SEU/MCU at Various Locations: Correlation and Analyses Based-On MUSCA SEP^3," *IEEE Transactions on Nuclear Science*, vol. 60, no. 4, pp. 2418–2426, 2013.

[32] G. Hubert and A. Cheminet, "Radiation Effects Investigations Based on Atmospheric Radiation Model (ATMORAD) Considering GEANT4 Simulations of Extensive Air Showers and Solar Modulation Potential," *Radiation Research*, vol. 184, no. 1, pp. 83–94, 2015.

[33] L. Artola *et al.*, "In Flight SEU/MCU Sensitivity of Commercial Nanometric SRAMs: Operational Estimations," *IEEE Transactions on Nuclear Science*, vol. 58, no. 6, pp. 2644–2651, 2011.

[34] M. C. Espirito-Santo, P. Goncalves, M. Pimenta, P. Rodrigues, B. Tome, and A. Trindade, "Applications of GEANT4 in astroparticle experiments," *IEEE Transactions on Nuclear Science*, vol. 51, no. 4, pp. 1373–1377, 2004.